Accepted Manuscript

Experimental and numerical study of the bending strength of natural fibre composite structural channel sections

M.R. Bambach

PII: S0263-8223(18)31508-3
DOI: https://doi.org/10.1016/j.compstruct.2018.11.031
Reference: COST 10396

To appear in: *Composite Structures*

Received Date: 23 April 2018
Revised Date: 23 October 2018
Accepted Date: 13 November 2018

Please cite this article as: Bambach, M.R., Experimental and numerical study of the bending strength of natural fibre composite structural channel sections, *Composite Structures* (2018), doi: https://doi.org/10.1016/j.compstruct.2018.11.031

Experimental and numerical study of the bending strength of natural fibre composite structural channel sections

M.R.Bambach
School of Civil Engineering, The University of Sydney, NSW 2006, Australia
mike.bambach@sydney.edu.au, T +61 2 9351 2193, F +61 2 9351 3343

ABSTRACT

Increasing awareness of environmental concerns is leading a drive towards more sustainable structural materials for the built environment. Natural fibres such as flax and jute have increasingly been considered for fibre-resin composites, with a major motivation for their implementation being their notable sustainability attributes. This paper is part of an ongoing effort by the author to demonstrate the structural properties of primary structural elements and members fabricated from natural fibre composites of flax and jute. Previously the structural properties of flat plates, plain channel sections and channel sections with complex stiffeners were investigated under pure compression. This paper presents investigations of channel sections with complex stiffeners under pure bending. A series of sixteen channels with varying geometries, complex stiffener arrangements and composite thicknesses were tested in pure flexure. Material tests indicated that the mean tensile elastic stiffness and strength values were 6,386 MPa and 55.1 MPa for flax, and 6,941 MPa and 62.1 MPa for jute. The experimental results indicated that flexural failure of the channel sections was governed by tensile fracturing. The ultimate moment capacities varied from 1.043 to 1.501 kNm for four-layered composites, and 2.184 to 2.511 kNm for six-layered composites. The analytical models predicted the experimental ultimate moment capacities well, with a mean and coefficient of variation of the test to predicted ratio of 0.97 and 0.06, respectively. Finite element models used progressive damage analysis via stress-based damage initiation models and damage evolution laws, to replicate the tension fracture failure mode of the channels. The numerical models

predicted the experimental ultimate moment capacities well, with a mean and coefficient of variation of the test to predicted ratio of 0.99 and 0.06, respectively.

KEYWORDS: natural fibre composites, flax, jute, channels, bending, flexure, finite element

1. INTRODUCTION

Public concerns about the environment, climate change, energy consumption and greenhouse gas emissions are driving demand for the use of sustainable materials in the built environment. There has been substantial attention given to the use of natural fibres in fibre-reinforced plastics in recent decades, where such fibres may be combined with thermoset or thermoplastic polymers to create natural fibre composites. Such natural fibre composites have particularly been identified for their favourable sustainability properties, including for example: renewable resource; carbon sink; short growth cycle time; low herbicide requirements due to rapid growth; low energy production; recyclable; biodegradable; and low hazard manufacturing and composite handling and working [1-7]. Much of this research has been from a materials science standpoint, assessing materials aspects such as fibre processing techniques, composite fabrication methodologies, matrix materials and their effects on the mechanical properties [8-13]. This research has indicated that composites consisting of natural fibres have general characteristics similar to their synthetic fibre counterparts, such as glass and carbon, however have comparably low intrinsic mechanical properties [2-13]. As a result, identifying structural applications such as those in civil infrastructure have thus far been limited [14-22].

Recently, the author has undertaken to demonstrate the structural properties of primary structural elements and members fabricated from natural fibre composites of flax and jute, including: flat plates and plain channel sections in pure compression [23], and channel sections with complex stiffeners in pure compression [24]. This paper extends these studies to investigate flax and jute fibre composites in pure bending. It is demonstrated that while the failure modes of the previous members in compression were dominated by elastic local buckling and compression matrix failure, the present failure modes in pure flexure are dominated by tension fracture. The stiffened channel sections were previously demonstrated to have compression capacities suitable for light structural applications such as residential building framing [24]. An aim of the present study is to determine if such channel sections are suitable for resisting the bending loads that such framing members undergo as a result of lateral wind loading.

Initially a series of sixteen experiments of flax and jute fibre composite structural channel sections subjected to pure (four-point) bending is described. An analytical method developed previously for compression [23,24] is then extended to the case of flexure. Finally, finite element analyses are described which demonstrate the suitability of progressive damage analysis to predict the bending capacity.

2. EXPERIMENTAL METHODS

2.1 Composite fabrication

Two different natural fibres were investigated in the present study; flax and jute. The flax and jute fabrics were commercially produced for fibre-resin composite fabrications by Composites Evolution; Biotex Flax 400g/m^2 2x2 Twill weave and Biotex Jute 400g/m^2 2x2 Twill weave. The 2x2 Twill weave is a generic pattern consisting of bi-directional yarns woven over-over-under-under, where the yarns are perpendicular (i.e. 0º/90º). The fabrics use a low-twist yarn. Nominal density, tensile strength and modulus values for the flax were; 1.5g/cm^3, 500MPa and 50GPa, and for the jute were; 1.46g/cm^3, 400MPa and 40GPa. The commercial bulk laminating epoxy resin Kinetix R240 with H126 (fast) hardener was used for all composite fabrications, with density 1.1g/cm^3 and measured (neat) compression ultimate stress of 105.3MPa, tension ultimate stress of 33.1MPa and tension ultimate strain of 0.8%. The epoxy is a room temperature out-of-autoclave cure epoxy resin that does not require heat input to cure. The manufacturers' technical data for the fabrics and epoxy are summarised in Appendix A. The channels were fabricated with a hand layup technique whereby each layer of fabric was wetted out with resin using a paint brush and roller. The fabric 0º direction was manually aligned with the longitudinal direction of the mandrel. The fabrics were laid over a mandrel and held under a full vacuum during a cure time of a minimum of 5 hours in a constant temperature room at 25ºC, as per the manufacturers recommendation. Due to laboratory scheduling arrangements, the fabricated channels were stored at room temperature for a minimum of one month prior to testing.

Fibre volume fractions were estimated using the mass of fabric prior to fabrication, the mass of composite after fabrication, and the constituent densities. The fabrication technique generated consistent fibre volume fractions, and for all specimens the mean and standard deviations of the fibre volume fractions were; 39.6% and 1.4% for flax, and 37.0% and 2.2% for jute.

2.2 Material properties

Tension material test specimens were cut from the flat portions of untested flax and jute channel specimens of four fibre layers in accordance with ISO 527 [25]. Tension specimens were cut at 0º and 45º to the channel longitudinal dimension so as to establish the uniaxial tension and in-plane shear strengths of the [0/90] composites, respectively. In the previous study [24], compression material tests of nominally identical flax and jute channel sections (using the same constituent materials and fabrication procedures as the present study) were undertaken, and these values were used in the present study for the uniaxial compression material properties. Mean material properties are summarised in Table 1 and exemplar tension material stress-strain curves are provided in Fig 1.

It is noted that the measured tension strengths indicated in Table 1 are relatively low compared with an estimate made with the rule of mixtures. For example, the jute composite has a mean tension strength of 62.1MPa, while the nominal fibre and matrix strengths are 400MPa and 105.3MPa, respectively. Using the rule of mixtures the estimated tension strength of the composite is 140MPa. There are several possible reasons why the measured strengths are relatively low:

a) the twill weave and vacuum assisted fabrication technique can result in voids in the matrix
b) the natural fibres contain lumens and sometimes the resin cannot penetrate inside the lumens
c) the manufacturers' data for the fibre strength of 400MPa was used for the rule of mixtures estimate, however it is unclear if this value is for a single elementary fibre or for the yarn
d) while the manufacturers' data indicates the yarn is low-twist, the twist is not zero and during tension the twist angle will change
e) the yarn consists of elementary fibres which may move relative to each other under tension

While the mechanical properties of the fabricated composites are relatively low, the measured jute value of 62.1MPa is reasonably consistent with the manufacturers' typical mechanical properties, being 59MPa tension strength for vacuum infused fabrication with an unsaturated polyester matrix (Appendix A).

2.3 Channel specimens

Flax and jute fibre-resin composite channels were fabricated with nominal geometries of web depth 100mm, flange width 50mm and 650mm length. Two different channel thicknesses of 4 and 6 fibre layers were fabricated for each of the different fibre types. In the previous study [24], structural optimisation of the channel section geometry was demonstrated with the inclusion of flange edge stiffeners and intermediate flange and/or web stiffeners. Based on these previous experimental and analytical optimisation results [24], several optimised shapes were considered for the present study, including: one intermediate web stiffener (Figure 2a,b), two intermediate web stiffeners (Figure 2c,d), and two intermediate web stiffeners with one intermediate flange stiffener (Figure 2e,f). All specimens contained flange edge stiffeners. For each different intermediate stiffener arrangement, two different sized flange edge stiffeners were used. For all configurations (Figure 2a to f) the smaller thickness was tested (4 layers of flax or jute), and for the configuration of two intermediate web stiffeners with one intermediate flange stiffener (Figure 2e,f) the larger thickness was additionally tested (6 layers of flax or jute).

The different stiffener configurations were fabricated by fixing 12mm diameter half-rounds to the mandrel at specific locations, the mandrel being two 50mm x 50mm steel square hollow (SHS) sections with external corner radius of 6mm. An example mandrel and resulting channel section is exemplified in Figure 3. A split mandrel was required to facilitate extraction of the mandrel after curing. It is noted that 2mm shim was placed between the SHS mandrel members to assist extraction, thus the nominal channel internal web depth was 102mm. For the specimens with two intermediate web stiffeners, the rounded corners of the SHS resulted in a small central stiffener, as some fabric and epoxy was drawn into this space (Figure 3a). This was an unintended artefact of the use of a split mandrel. The stiffeners were centrally located for all elements with one stiffener, and located at the quarter points for elements with two stiffeners (Figure 3b).

The channels were fabricated with an approximate length of 650mm. The ends did not require trimming due to the test setup used (described in the next section). The flange edge stiffeners were fabricated with approximate length of 40mm, then following curing were trimmed to nominal dimensions of 15mm or 25mm using a high speed rotary tool (Dremel brand), with a carbide cutting wheel. The measured channel geometries are tabulated in Table 2. Exemplar channel specimens are shown in Figure 4.

2.4 Channel section bending tests

The channels were tested in pure flexure using a traditional four-point bending arrangement. The distance between the support points was 600mm, the distance between the support and loading points was 125mm, and the length of the pure flexure region was 350mm (Figure 5a).

A steel restraint system was clamped to the composite channels between the support and loading points at both ends to prevent localised flange distortions, web crippling and/or shear failures, restricting the sections to fail in the pure flexure region. The restraint system consisted of two steel channel sections placed over the top and bottom flanges, connected with threaded rods to clamp onto the composite channel sections. Steel rectangular hollow sections (RHS) were inserted inside the composite channels. Additionally, several steel packing plates were inserted between the composite channels and steel channels, while small bolts were inserted through threaded holes in the steel channels and tightened against these packing plates, so as to fully restrain each of the flange and web elements of the composite channels between the steel channel and the steel RHS insert (Figure 5b). Failure occurred in the pure flexure region in all tested channels, demonstrating that the steel restraint system was effective in precluding localised failures outside the pure flexure region.

An inclinometer was clamped to each steel restraint system to measure the applied end rotations. The channels were loaded in vertical displacement control at a speed of 1mm/min. The channel lengths in the pure flexure region were short enough so as to preclude flexural-torsional buckling, which was confirmed by the experimental results observed, such that the pure section bending moment capacity was established.

3. EXPERIMENTAL RESULTS

3.1 Moment-curvature results

The machine vertical applied load was converted to applied moment from the geometry of the test setup, and likewise the inclinometer results were converted to curvature. An exemplar moment-curvature plot with photographs taken throughout the bending test is shown in Figure 6, several exemplar results are plotted in Figure 7 with photographs of the specimens nearing ultimate, and ultimate moments are tabulated in Table 2.

3.2 Failure modes

The results demonstrated a predominantly linear-elastic response, with some softening prior to failure. Failure was governed by tensile fracturing, initiated in the pure flexure region immediately adjacent to the load point at one end. The fracture initiated in the tension flange and progressed upwards into the web, and thence into the compression flange (Figure 8a). In four jute channels the fracture propagated completely through the compression flange, separating the channel into two pieces (Figure 8b). These tensile fracture failures were sudden and brittle in nature, with only a small amount of softening prior to failure, as evidenced in the moment-curvature plots (Figure 7).

The softening resulted from a small amount of compression flange buckling, and matrix damage as the material failure stress was approached, resulting in a reduction in the bending stiffness. Small compression flange buckling is evidenced in the photographs in Figure 7 for channels 1 to 4. A reliable technique to measure the compression flange buckling displacement was not found, as difficulties were encountered in the mounting of displacement transducers from relative movements between the mount base and the flange edge that were unrelated to buckling. Generally, all four layered specimens underwent some compression flange buckling, which was more pronounced for the channels with smaller flange edge stiffeners and without flange intermediate stiffeners.

3.3 Comparisons between different channel sections

The moment capacities indicated that despite the jute composite having a slightly higher uniaxial tension stress (Table 1), the flax channels had slightly higher moment capacities. This may result from the fact that the flax composite has greater ductility than the jute (Figure 1), allowing the flax channels to continue resisting load while undergoing matrix damage for longer.

For comparisons of structural efficiencies between different flange and web intermediate stiffener arrangements, and different thicknesses, the average ultimate stress is a better measure than ultimate moment, since the addition of stiffeners also involved the addition of extra material. The average ultimate stress (f_{ult}) was calculated from the ultimate moment in the test (M_{test}) and the full section bending properties, Equation 1, where y_{full} is the full section distance from the neutral axis to the extreme bending fibre, and I_{full} is the full section second moment of area (where the designation of 'full' refers to the gross section, as opposed to the effective section discussed in the next section). These values are tabulated in Table 2. The full section second moments of area were calculated using the cross-section analysis software ThinWall [26].

$$f_{ult} = \frac{M_{test} y_{full}}{I_{full}} \tag{1}$$

Compared with one web stiffener, the addition of a second web stiffener resulted in a very small increase in average ultimate stress for both the flax and jute channels. The addition of the second web stiffener was designed to increase the strength via restricting compression buckling of the web, however web buckling did not occur in the single web stiffened channels, thus the effect of adding the second stiffener was negligible.

Compared with no intermediate flange stiffeners, the addition of an intermediate flange stiffener decreased the average ultimate stress for both the flax and jute channels. Since the bottom flange is in pure tension, and is the location of the initiation of tension fracture, this may result from the flange stiffener acting as an inclusion or disturbed region, weakening the flange and precipitating earlier fracture. This was exacerbated by the fact that the stiffener was on the outside of the section, such that the extreme fibre of the section (and thus the location of maximum stress during bending) was the outer fibre of the stiffener. The addition of the stiffener to the flat flange element was designed to increase the strength via restricting compression buckling of the flange, however it is apparent that it may actually weaken the section as a result of earlier onset of tension fracture.

This moment reduction was especially notable in the four layer jute channels with two web stiffeners and intermediate flange stiffeners (Table 2), to the extent that these results seemed to be outliers to the rest of the data. To investigate further, tension material specimens were cut from these two jute channels (from inside the steel restraints, post- bending test) and tested in uni-axial tension, indicating a tension strength of 51.9MPa, notably lower than the average jute value of 62.1MPa. It is likely that there was a manufacturing defect in these two channels which were fabricated together (for example incorrect epoxy resin mix, incomplete vacuum pressure, etc, which occurs sometimes when composites are fabricated by hand layup).

While there were differences in the average ultimate stress values between different stiffener arrangements as noted above, these differences were small (except for the two outlier jute channels with lower material strengths). The highest average ultimate stresses were achieved in the thicker channels for both flax and jute. While they may have been negatively affected by the inclusion of intermediate flange stiffeners, the positive effect of the thickness in stabilising the section against compression flange buckling resulted in an overall small positive effect on the strength.

4. ANALYTICAL ANALYSIS

The effective width analytical method was developed to predict the post-buckling strength of thin-walled elements, predominantly steel, and forms the basis for the design of cold-formed steel members in several international structural specifications. In the previous investigations by the author, the method was applied to natural fibre composites to predict the compression capacity of plates and channel sections [23,24]. Relatively good agreement with experiments was observed, due to the realistic depiction of the post-buckling mechanics of thin elements; the assumption is made that the buckled regions become ineffective in carrying load, redistributing the stress to the unbuckled regions, which resist the load until some limit stress is reached (e.g. the yield stress for steel). The limit stress in compression for the composites was taken as the compression matrix failure stress (f_{uC}, Table 1).

For design purposes, the method requires a prediction of the buckling stress and an equation that relates the buckling stress to the effective width that ensues at the limit state (the strength equation). The strength equation for natural fibre composites was derived empirically [24] and given by Equations 2 and 3, where ρ is the element effectiveness ratio, λ is the element slenderness and f_{cr} is the element elastic buckling stress;

$$\rho = \frac{1.28}{\lambda^{1.5}} \leq 1 \tag{2}$$

$$\lambda = \sqrt{\frac{f_{uC}}{f_{cr}}} \tag{3}$$

The application to sections in bending is identical, except that only the regions of the section in compression are susceptible to buckling. The elastic bucking and effective width equations used in the cold-formed steel structural specification AS/NZS 4600 [27] were followed exactly, as was done in the previous compression design analysis [24]. The exception being that the steel strength equation was replaced with the natural fibre composite strength Equation 2. In pure bending, the elastic buckling coefficient for the web is 24 (rather than 4 for pure compression). The compression flange is in uniform compression for both load cases of pure bending and pure compression, thus the flange analysis follows exactly as previously [24]. In [24] the method is fully described, and several worked examples are provided in the supplementary to the article, thus readers are referred to that article for further details. For the natural fibre composite channels in bending the effective width concept is demonstrated in Figure 9. The compressed portion of the web is shown as fully effective in Figure 9, since this was calculated to be the case for all composite channels in the present study.

Having established the effective section (Figure 9), the effective section properties (I_{eff}, y_{eff}) were calculated using the cross-section analysis software ThinWall, and used in place of the full section values, Equation 4, to analytically predict the moment capacity (M_{Apred}). The effective section properties and the calculated moment capacities are tabulated and compared with the experimental values in Table 2. An example calculation is shown in Appendix B.

$$M_{Apred} = \frac{f_{uT} I_{eff}}{y_{eff}} \qquad (4)$$

While the analytical method does not incorporate the effects of matrix damage, the use of the measured ultimate tensile stress (f_{uT}, Table 1) produces good agreement with the experiments, with an average test/predicted ratio of 0.97 and coefficient of variation of 0.06. It is interesting to note that the flax and jute channels with 6 layers were calculated to be fully effective, which indicates that the compression flange did not undergo compression buckling. This result is in agreement with the experimental results, where despite the presence of flange intermediate stiffeners (which were demonstrated to weaken the tension flange), these channels reached the highest average ultimate stress. These channels could be considered as the most structurally efficient geometries of those considered in this study.

5. FINITE ELEMENT ANALYSIS

5.1 General

The finite element model approach did not consider the fibres and the resin as discrete and separate elements, and model them separately with their own individual material properties. Rather, the model used a macro-approach, whereby the fibres and resin are modelled as a composite fibre-resin matrix with a single set of mechanical properties assigned to this matrix. The material properties of the composite fibre-resin matrix were carefully ascertained in accordance with ISO-specified procedures, and the models were prepared in accordance with typical practice for modelling fibre-resin composites. The material properties of the composite fibre-resin matrix used in the models are provided in complete detail in Appendix C.

The commercial software ANSYS Workbench version 18.2 [28] was used for the finite element modelling. The channel sections were generated from the measured geometries, and exemplar models are shown in Figure 10a. Parametric studies indicated a mesh size of 5mm was suitable, however in order to accurately articulate the corner radii of the internal stiffeners, a mesh size of 3mm was used for all models (Figure 10b). Four-node shell elements with six degrees of freedom per node were used for the mesh. In accordance with the experimental setup and results, the segments of the channels between the load and support points were fully restrained with the steel restraint system, thus these were not required to be modelled. The full 350mm pure flexure length of the channels between the loading points was modelled, and both ends were loaded with enforced pure rotations about the major axis. The reaction moments at the ends were extracted from the results, and the enforced rotation magnitude was increased until such time as the moment reaction decreased beyond the peak value (this magnitude of rotation was defined through several trial values). A large-displacement Newton-Raphson non-linear solution scheme was used, with 10 end rotation steps manually defined and up to 100 sub-steps allowed within each defined step.

5.2 Material properties

The material models in ANSYS are capable of defining different material properties for each individual fibre layer in a composite layup. Since the present composite layups consisted of multiple layers where each individual layer in the layup had the same fibre orientation [0/90], all layups were modelled as a single layer with a thickness equal to the measured total thickness of the layup. The material was defined as elastic orthotropic, with identical values in both in-plane directions (due to the 0/90 fibre orientation) based on the measured properties (Table 1), and nominal values of 10% of the in-plane values in the through-thickness direction.

In order to estimate failure and thereby predict peak moment values, a progressive damage analysis via stress-based damage initiation models and damage evolution laws was used. Stress limits in tension and compression were defined by specifying the measured failure stress values in tension and compression (f_{uT} and f_{uC} in Table 1). The stress limits in shear were defined by specifying the failure stress values measured in the tension material tests at 45º to the fibre direction (f_{uS} in Table 1). Strain limits were set at 10% such that strain limits were not invoked in the damage initiation model. The default values for the Tsai-Wu constants were used and the Hashin damage initiation criteria was invoked.

Damage evolution was defined with the continuum damage mechanics model in ANSYS. This models the evolution of damage both within an element and throughout the mesh, and is based on energy dissipation, as opposed to the alternative property degradation method which is an instant stiffness reduction method. While this damage evolution model is more robust than stiffness degradation, it requires the definition of material properties that are difficult to quantify. These include the energy dissipated per unit area from: tensile fibre damage, compressive fibre damage, tensile matrix damage, and compressive matrix damage. Each of these values also has an associated damping constant, which dampens the damage accumulation and is designed to reduce convergence issues associated with material softening. The energy dissipated per unit area (G) is defined as [28];

$$G = \int_0^{U_{fe}} \sigma_e dU_e \tag{5}$$

where σ_e is the equivalent stress, U_e is the equivalent displacement, and U_{fe} is the ultimate equivalent displacement where material stiffness is completely lost. For a simple uni-axial stress state, the equivalent values are equal to the actual (uni-axial) values, and the actual displacements are defined as;

$$U_e = \varepsilon L_c \tag{6}$$

where ε is the uni-axial strain and L_c is the length of the element in the direction of the stress/strain. Thus for a uni-axial stress state, the energy dissipated per unit area is calculated by integrating the material stress-(strain x L_c) curve up to material fracture. However, material data was not available for the flax and jute composites differentiating between fibre- and matrix-dominated modes, nor material compression stress-(strain x L_c) data up to complete failure. All energy dissipation constants were therefore assumed to be equal to the uni-axial value for tension, which was derived by integrating the flax and jute measured material stress-(strain x L_c) curves (Figure 1). Since all finite element models used a constant element size of 3mm, L_c was taken as 3mm. Accordingly, the calculated energy dissipated per unit area values for flax and jute were: 1.81 N/mm and 1.08 N/mm, respectively. A nominal value for damping of 10% was used for all cases. The complete set of values used for the flax and jute composite material definitions are tabulated in Appendix C.

5.3 Finite element analysis results

The finite element models replicated the moment-curvature response well, with a linear-elastic response up to the initiation of damage, some softening as damage progressed, then failure indicated as a reduction in the bending moment resistance. An exemplar finite element moment-curvature response is compared with the experimental curve in Figure 11. It is noted that the finite element models demonstrated slightly stiffer responses than the tests, likely due to small movements of the composite channels inside the steel restraints in the tests. An exemplar deformed shape at the ultimate state is shown in Figure 12. It is noted that few solution steps were required in the linear-elastic region, however in the highly non-linear damage phase many more steps were required to correctly identify the softening and failure path (Figure 11b).

The damage evolution replicated the experimental damage progression well, where damage initiated in the tension flange, then the damaged region grew across the flange and into the web, while the material softened to the point that the section moment resistance began decreasing. With respect to the applied end rotation, the damage progressed quickly to the point of failure (moment reduction), as was found in the experiments. A typical failure progression is shown in Figure 13.

Despite using the tension value for the energy dissipated per unit area (G) in compression, the progressive damage model performed reasonably well. This may have resulted from the fact that the failure was in fact tension dominated, thus the compression damage values were not especially relevant. The moment capacity results from the finite element models are compared with the experimental moment capacities in Table 2 ($M_{test}/M_{FEpred1}$). The strength of the jute composite channels was predicted well, with all values within 8% of the experimental ones except for the two outliers with possible manufacturing defects discussed previously. For these two defect channels, the measured reduced material failure stress of 51.9MPa was input into the models, which improved their prediction.

The strength of the flax channels were conservatively predicted in all cases, with results up to 19% lower than the experimental values ($M_{test}/M_{FEpred1}$). Since all material values were accurately defined based on measured values except for the energy dissipated per unit area (G), this value was empirically adjusted to match the experimental moment capacities. Trial and error found that the energy dissipated per unit area was required to be multiplied by three in order to replicate the ultimate moments. When three times the energy dissipated per unit area (i.e. G_{flax} = 5.43 N/mm) was used for all flax channels, the moment capacities matched the experimental values well, and were all within 6%. These values are referred to as $M_{test}/M_{FEpred2}$ in Table 2.

Using the unadjusted jute models and the adjusted flax models ($M_{test}/M_{FEpred2}$), the moment capacities compared well with the experimental capacities, with a mean test/predicted ratio of 0.99 and standard deviation of 0.06 (Table 2). Except for one outlier, the maximum error was 8%. These results indicate that using the measured material properties for the elastic properties and the stress limits, and the calculated energy dissipated per unit area values from Equations 5 and 6 based on the measured tension material properties, provides reasonable agreement with experimental values. However, the energy dissipated per unit area may need to be empirically adjusted in order to obtain excellent agreement. Care should be taken in extrapolating these conclusions to loading situations where the failure is not tension dominated, as the use of the tension energy dissipated per unit area value may not be appropriate for such situations. It is noted that the damage progression is not especially sensitive to the magnitude of the energy dissipated per unit area value; an increase of 2 times resulted in an average increase in moment capacity of 8%, while an increase of 3 times resulted in an average increase in moment capacity of 14%.

6. APPLICATION IN RESIDENTIAL STUD WALLS

In the previous studies by the author on natural fibre channel sections in compression [23,24], the compression capacities were noted to be only suitable for light structural applications, due to their relatively modest strength. A potential light structural application identified was as stud columns in residential stud walls, and comparisons with steel stud columns demonstrated suitable capacities. Flax and jute channels fabricated with exactly the same dimensions and fibre thicknesses as those in the present study had compression capacities between 27kN and 69kN, while a commercially produced load-bearing steel stud had a compression capacity of 41kN (Rondo channel section with a nominal web depth of 92mm, flange width of 33mm and thickness 1.15mm from 300MPa steel.).

This same steel stud has a moment capacity of 1.26kNm (as reported by the manufacturer Rondo), while the flax and jute channels had moment capacities between 1.04kNm and 2.51kNm. This indicates that many of the natural fibre channels had compression and bending capacities comparable with, or in excess of, commercial steel channels used as residential stud wall columns.

To quantify the structural suitability of the present natural fibre channels for residential applications, the Australian design criteria for timber-framed residential buildings was applied (AS 1720 [29]). Stud wall columns must satisfy the combined compression and bending interaction Equation 7, where N^* is the design compression load (from gravity loads), M^* the design bending moment (from lateral wind loads), ϕN_u is the compression capacity and ϕM_u is the bending capacity. The capacity factors are derived from reliability analyses, and the compression capacity factor was calculated as 0.75 in [24], and following a similar procedure was calculated as 0.8 for the moment capacities in the present study.

$$N - M_{limit} = \frac{N^*}{\phi N_u} + \frac{M^*}{\phi M_u} \leq 1 \tag{7}$$

To characterise the compression and bending loads the procedures in [29] were followed, with several assumptions, including; a wind region of N3 (this is the second highest non-cyclonic wind category in Australia), 2.7m wall height, sheet roof, plasterboard claddings, 0.6m stud spacings, etc. Such assumptions result in design compression and bending loads of 8.8kN (N^*) and 0.41kNm (M^*), respectively. Using the compression test capacities from [24] (N_u), the bending test capacities in the present study (M_u), and the capacity factors of 0.75 and 0.8 respectively, the N-M_{limit} values for each of the flax and jute channels were calculated from Equation 7 and are tabulated in Table 2. Similarly, the procedures for assessing the lateral stiffness of the stud columns were followed, whereby a serviceability wind pressure was used with the measured E and I values of the channels (Table 2), to calculate the lateral deflection under service wind loads. The deflection limit for a

2.7m high wall is 18mm, and the calculated deflections are listed in Table 2 (*M defl*). The results in Table 2 indicate that all flax and jute channels satisfied the strength and stiffness limits for the particular assumed conditions for residential stud walls.

It should be noted that the above analyses consider only the structural suitability of natural fibre channels for residential stud walls. Clearly, there are many factors that would need to be addressed before natural fibre composites could be introduced into buildings, for example; fatigue-related matrix damage, column buckling, other loading types, connections, fire performance, environmental exposure and durability, etc., which were outside the scope of the present study.

7. CONCLUSIONS

Public concerns about the environment, climate change, energy consumption and greenhouse gas emissions have placed increasing demands for the use of sustainable materials in the built environment. Natural fibre composites such as those consisting of flax and jute fibres, may one day prove a viable and environmentally sustainable alternative to traditional building materials. The present study of natural fibre channels in pure bending complements previous studies of natural fibre channels in pure compression, and further demonstrates the structural properties of primary structural elements fabricated from flax and jute composites. Material tests indicated that the mean tensile elastic stiffness and strength values were 6,386 MPa and 55.1 MPa for flax, and 6,941 MPa and 62.1 MPa for jute. The ultimate moment capacities varied from 1.043 to 1.501 kNm for four-layered composites, and 2.184 to 2.511 kNm for six-layered composites. While these structural properties are modest, structural suitability for light structural applications such as residential load-bearing stud walls has been demonstrated. Combined axial compression and bending capacities were between 0.38 and 0.87, with no channels exceeding the design limit of 1.0. The suitability of the effective width mechanics model for analytically predicting their compression and bending strengths has been further demonstrated. The analytical models predicted the experimental ultimate moment capacities with a mean and coefficient of variation of the test to predicted ratio of 0.97 and 0.06, respectively. Finite element procedures for predicting their strength via progressive damage analysis have also been successfully demonstrated. The numerical models predicted the experimental ultimate moment capacities with a mean and coefficient of variation of the test to predicted ratio of 0.99 and 0.06, respectively.

8. REFERENCES

[1] Summerscales J, Dissanayake NPJ, Virk AS, Hall W. A review of bast fibres and their composites. Part 1 – fibres as reinforcements. Composites: Part A 2010;41:1329-1335.

[2] Summerscales J, Dissanayake NPJ, Virk AS, Hall W. A review of bast fibres and their composites. Part 2 - composites. Composites: Part A 2010;41:1336-1344.

[3] Ku H, Wang H, Pattarachaiyakoop N, Trada M. A review on the tensile properties of natural fibre reinforced polymer composites. Composites: Part B 2011;42:856-873.

[4] Yan LB, Chouw N, Jayaraman K. Flax fibe and its composites – a review. Composites: Part B. 2014;56:296-317.

[5] Pickering KL, Efendy MGA, Le TM. A review of recent developments in natural fibre composites and their mechanical performance. Composites: Part A 2016;83:98-112.

[6] Faruk O, Bledzki A, Fink H, Sain M. Biocomposites reinforced with natural fibres: 2000 – 2010. Progress in Polymer Science 2012;37:1552-1596.

[7] Dicker M, Duckworth P, Baker A, Francois G, Hazzard M. Green composites: A review of material attributes and complementary applications. Composites Part A 2014;56:280-289.

[8] Weclawski BT, Fan M, Hui D. Compressive behaviour of natural fibre composite. Composites: Part B 2014;67:183-191.

[9] Costa FHMM, D'Almeida JRM. Effect of water absorption on the mechanical properties of sisal and jute fibre composites. Polym Plast Technol Eng 1999;38(5):1081-94.

[10] Hargitai H, Racz I, Anandjiwala RD. Development of hemp fiber reinforced polypropylene composites. J Therm Comp Mat 2008;21:165-74.

[11] Oksman K. High quality flax fibre composites manufactured by the resin transfer moulding process. J Reinf Plast Comp 2001;20(7):621-7.

[12] Van de Weyenberg I, Ivens J, De Coster A, Kino B, Baetens E, Verpoest. Influence of processing and chemical treatment of flax fibres on their composites. Comp Sci Tech 2003;63:1241-46.

[13] Lefeuvre A, Bourmaud A, Morvan C, Baley C. Elementary flax fibre tensile properties: Correlation between stress-strain behaviour and fibre composition. Ind Crops Prod 2014;52:762-69.

[14] Dittenber D, GangRao H. Critical review of recent publications on use of natural composites in infrastructure. Composites Part A 2012;43:1419-1429.

[15] Yan LB, Chouw N. Crashworthiness characteristics of flax fibre reinforced epoxy tubes for energy absorption application. Mat Des 2013;51:629-40.

[16] Yan LB, Chouw N. Behaviour and analytical modelling of natural flax fibre reinforced polymer tube encased coir fibre reinforced concrete composite column. J Comp Mater 2013;47(17):2133-48.

[17] Mak K, Fam A, McDougall C. Flexural Behavior of Sandwich Panels with Bio-FRP Skins Made of Flax Fibers and Epoxidized Pine-Oil Resin. Journal of Composites for Construction 2015;19(6):04015005.

[18] Duigou AL, Deux JM, Davies P, Baley C. PLLA/flax mat/balsa bio-sandwich manufacture and mechanical properties. Appl Compos Mater 2011;18:421-38.

[19] Uddin N, Kalyankar RR. Manufacturing and structural feasibility of natural fiber reinforced polymeric structural insulated panels for panelized construction. Int J Polym Sci 2011;96:35-49.

[20] Shah DU, Schubel PJ, Clifford MJ. Can flax replace E-glass in structural composites? A small wind turbine blade case study. Composites Part B 2013;52:172–81.

[21] Corradi S, Isidori T, Corradi M, Soleri F. Composite boat hulls with bamboo natural fibres. Int J Mater Prod Technol 2009;36(1):73–89.

[22] Alvarez-Valencia D, Dagher HJ, Lopez-Anido RA, Davids WG, Gardner DJ, Center AC. Behavior of natural-fiber/thermoplastic sheet piling. ACMA-composites and polycon conference, January 2009, Tampa, Florida, USA; 2009.

[23] Bambach MR. Compression strength of natural fibre composite plates and sections of flax, jute and hemp. Thin-Walled Structures, 2017, 119:103-113.

[24] Bambach MR. Geometric optimisation and compression design of natural fibre composite structural channel sections. Composite Structures, 2018, 185:549-560.

[25] ISO 527-4:1997. Plastics – Determination of tensile properties. Part 4: Test conditions for isotropic and orthotropic fibre-reinforced plastic composites

[26] Papangelis JP, Hancock GJ. Computer analysis of thin-walled structural members. Computers & Structures, 1995, 56(1):157-176.

[27] AS/NZS 4600:2005. Australian/New Zealand standard: Cold-Formed Steel Structures, Standards Australia; 2005.

[28] ANSYS Mechanical APDL, Advanced Analysis Guide. SAS IP Inc, 17th ed.; 2016.

[29] AS 1720.3:2016. Australian Standard for Timber structures, Part 3: Design criteria for timber-framed residential buildings. Standards Australia, 2016.

NOTATION

B is the outside width of the channel section

D is the outside depth of the channel section

E_C is the compression elastic modulus

E_T is the tension elastic modulus

f_{cr} is the elastic buckling stress

f_{ult} is the average ultimate stress of the channel section

f_{uC} is the ultimate compression stress

f_{uS} is the ultimate shear stress

f_{uT} is the ultimate tension stress

FS is the internal flange stiffener

G is the energy dissipated per unit area

I_{eff} is the effective section second moment of area

I_{full} is the full (gross) section second moment of area

L is the overall length of the channel section

LL is the longer length flange edge stiffener

M_{Apred} is the analytically predicted moment capacity of the channel section

M_{FEpred} is the finite element predicted moment capacity of the channel section

M_{test} is the experimental moment capacity of the channel section

NA is the neutral axis

SL is the shorter length flange edge stiffener

U_e is the equivalent displacement

U_{fe} is the ultimate equivalent displacement where material stiffness is completely lost

WS is the web stiffener

y_{full} is the full section distance from the neutral axis to the extreme bending fibre

ε_{uT} is the failure strain in tension

λ is the slenderness factor

ρ is the effectiveness factor

σ_e is the equivalent stress

FIGURES

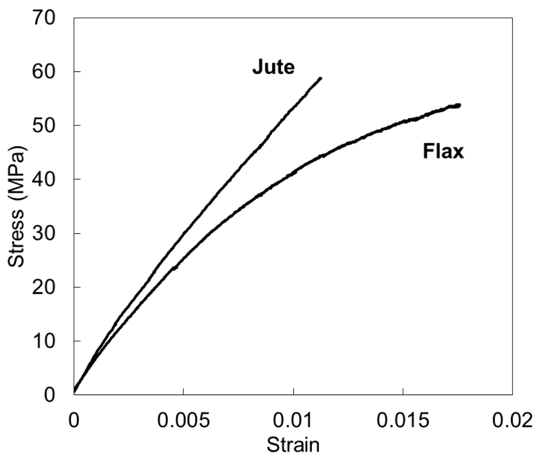

Figure 1: Measured uni-axial tension stress-strain curves (fibre volume fractions of 39% for jute, and 40% for flax)

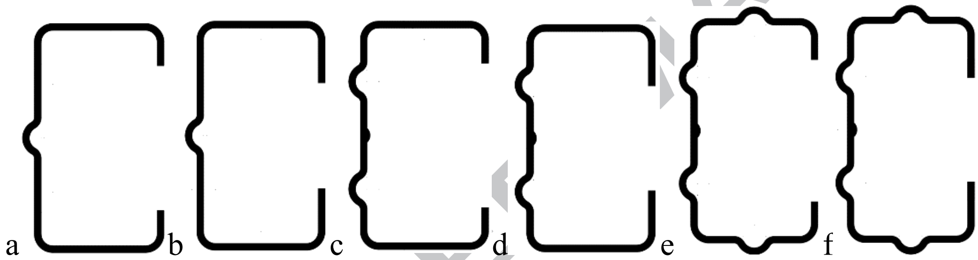

Figure 2: Channel section geometries

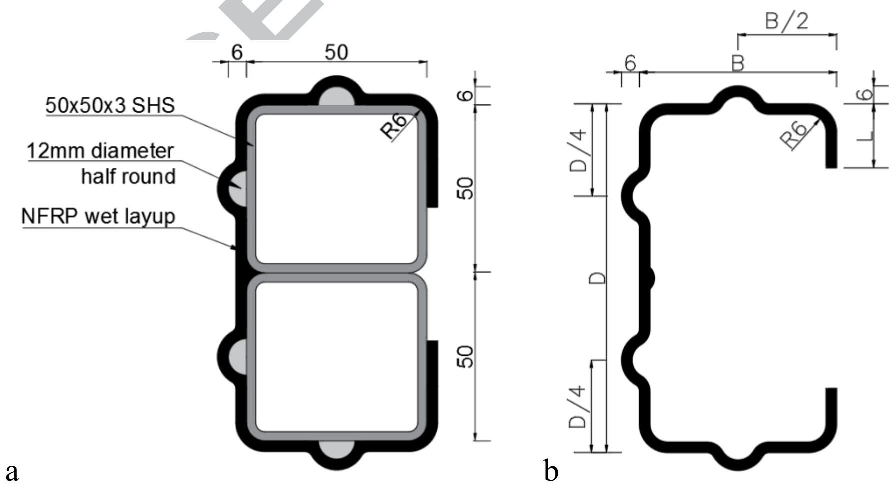

Figure 3: Channel fabrication; a) exemplar fabrication mandrel, b) resulting channel section (B, D, L are outside dimensions)

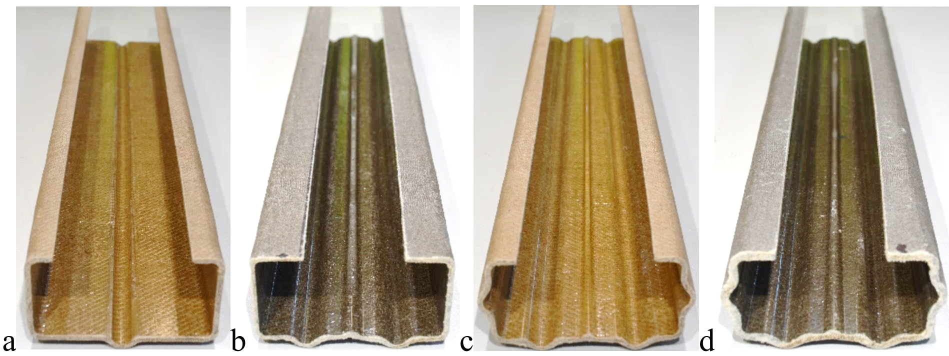

Figure 4: Exemplar composite channel specimens: a) 4 layered jute (type Figure 2a); b) 4 layered flax (type Figure 2d); 4 layered jute (type Figure 2e); 6 layered flax (type Figure 2f)

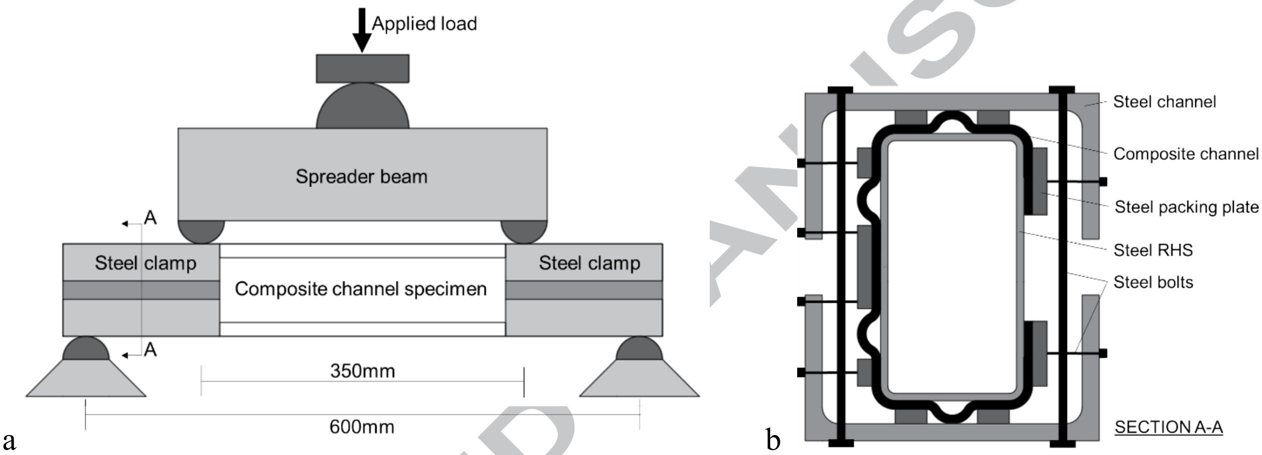

Figure 5: Experimental four-point bending setup; a) elevation, b) section

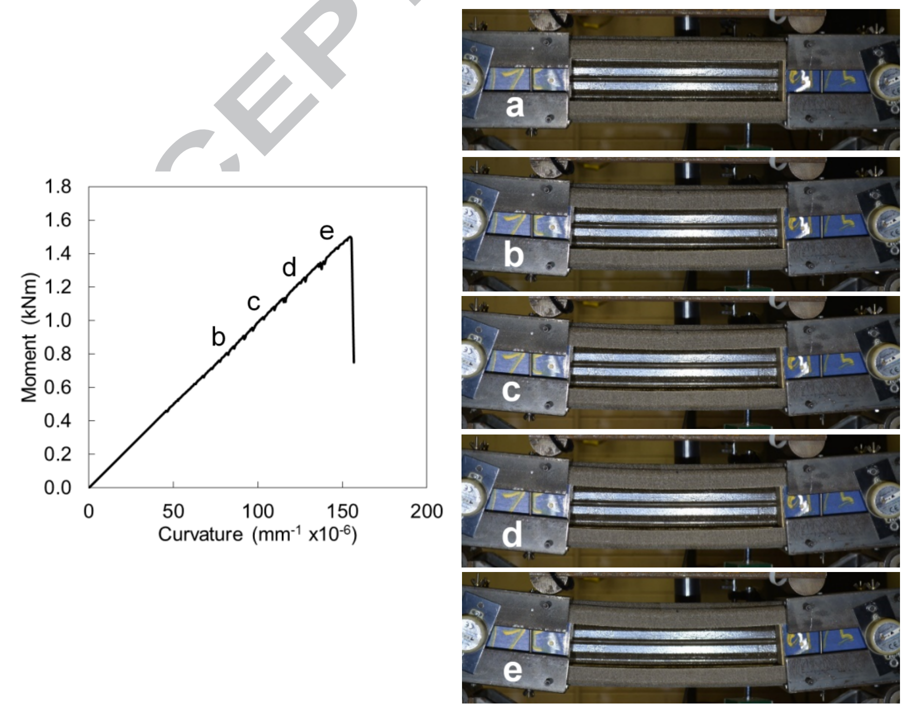

Figure 6: Exemplar moment-curvature response (flax 4 layers 2WS 1FS LL) with photographs at periodic intervals; a) 0kNm, b) 0.88kNm, c) 1.13kNm, d) 1.25kNm, e) 1.44kNm

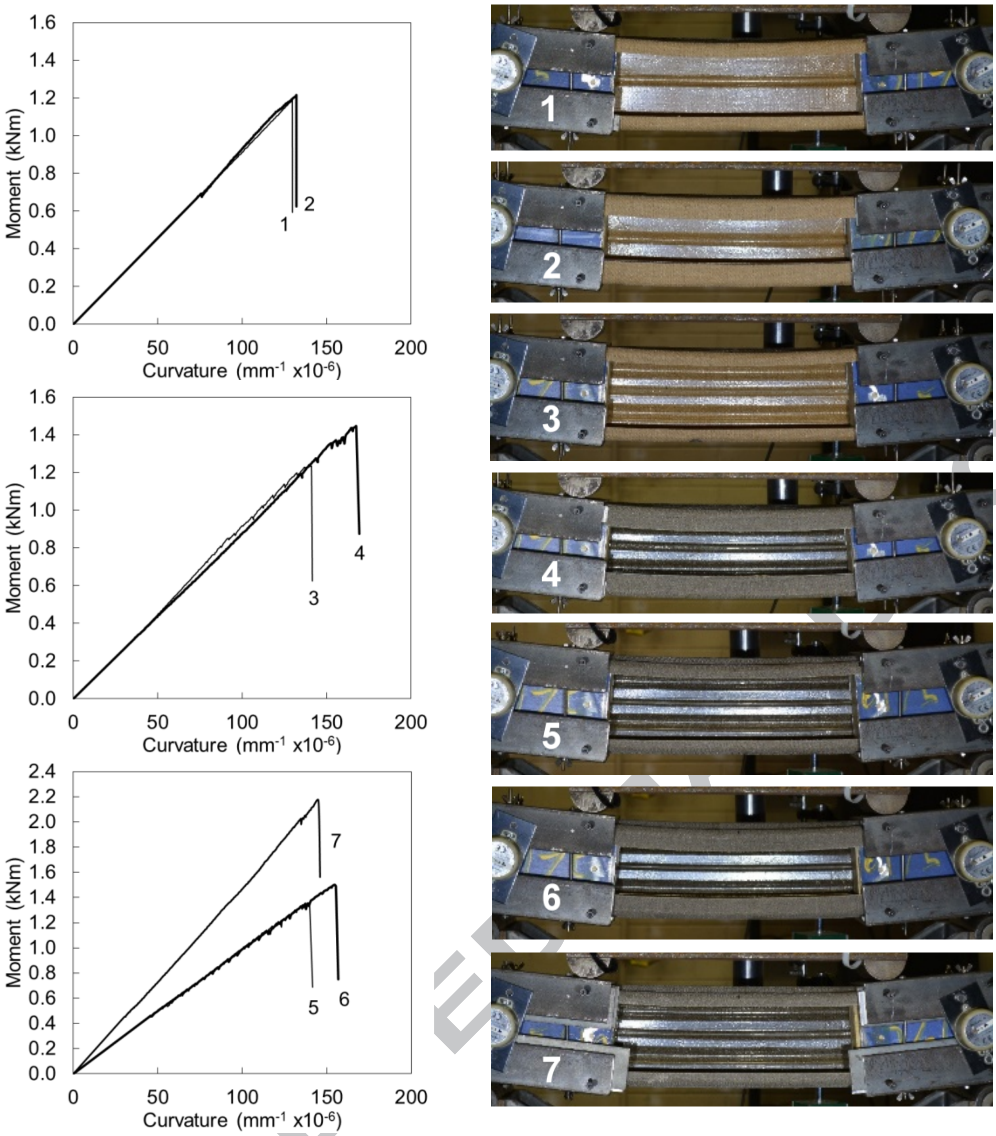

Figure 7: Moment-curvature responses of exemplar channels with photographs approaching the ultimate state; 1) jute 4 layers 1WS SL, 2) jute 4 layers 1WS LL, 3) jute 4 layers 2WS SL, 4) flax 4 layers 2WS LL, 5) flax 4 layers 2WS 1FS SL, 6) flax 4 layers 2WS 1FS LL, 7) flax 6 layers 2WS 1FS SL

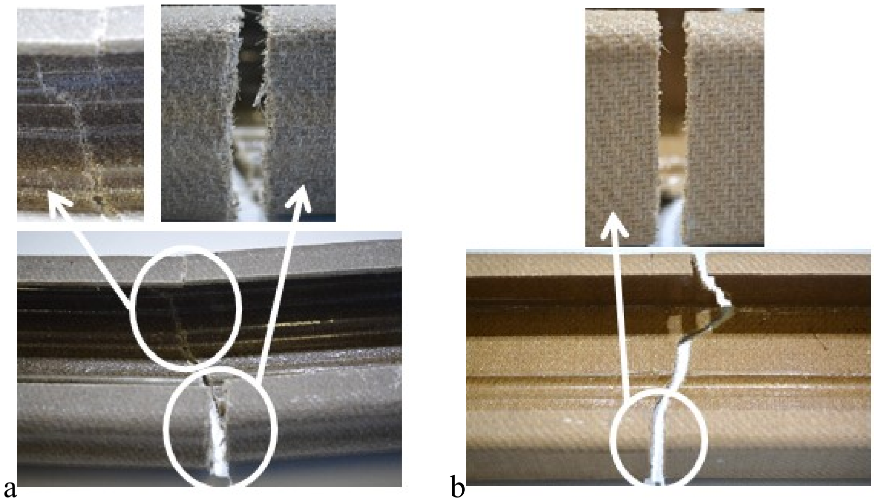

Figure 8: Exemplar failure modes (tension flange is the lower flange); a) 6 layered flax, b) 4 layered jute

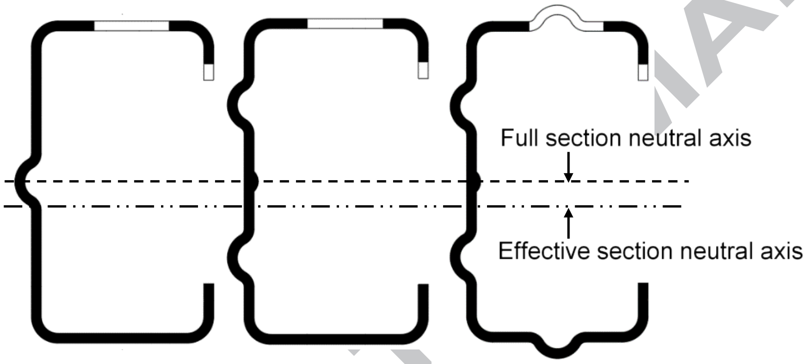

Figure 9: Exemplar effective widths (black areas) at the limit state, and the shift of the major axis bending neutral axis (towards the tension side) between the full section and the effective section

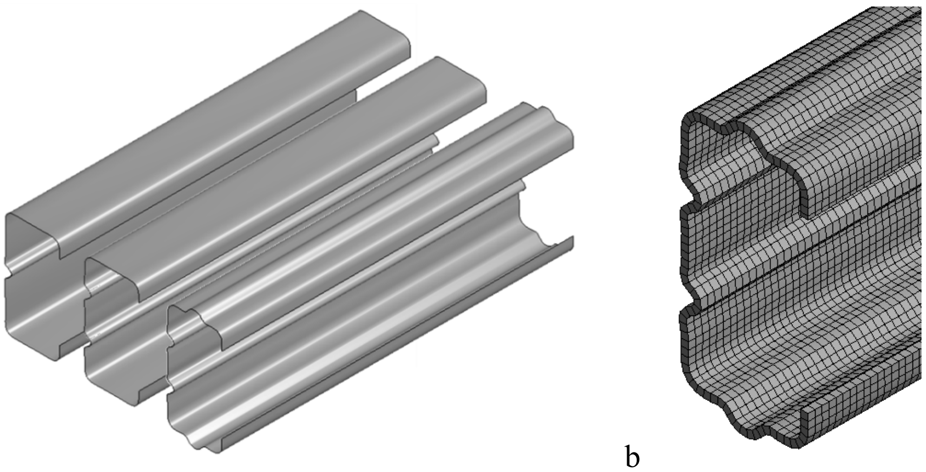

a b

Figure 10: ANSYS modelling; a) exemplar finite element model geometries, b) exemplar 3mm shell mesh used in all models

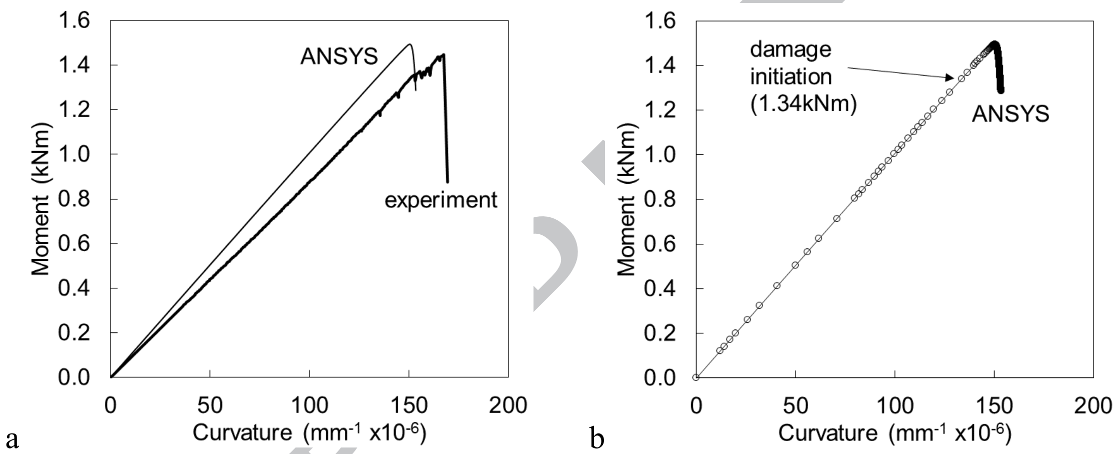

Figure 11: Finite element (ANSYS) solution for specimen flax 4 layers 2WS LL; a) comparison with experimental moment-curvature response, b) ANSYS solution points and damage initiation

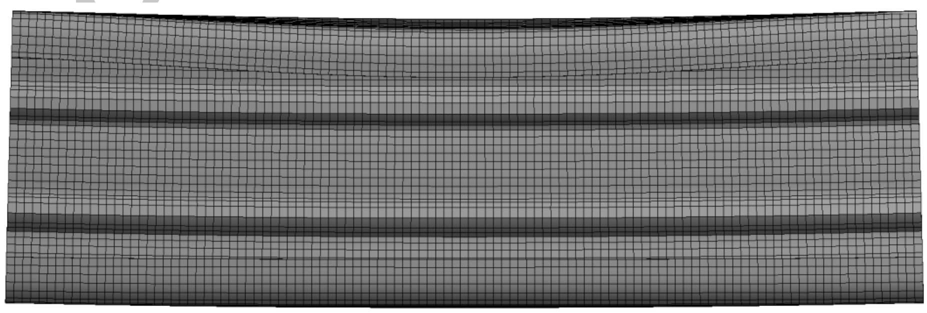

Figure 12: Exemplar deformation at the ultimate state (true scale); flax 4 layers 2WS SL

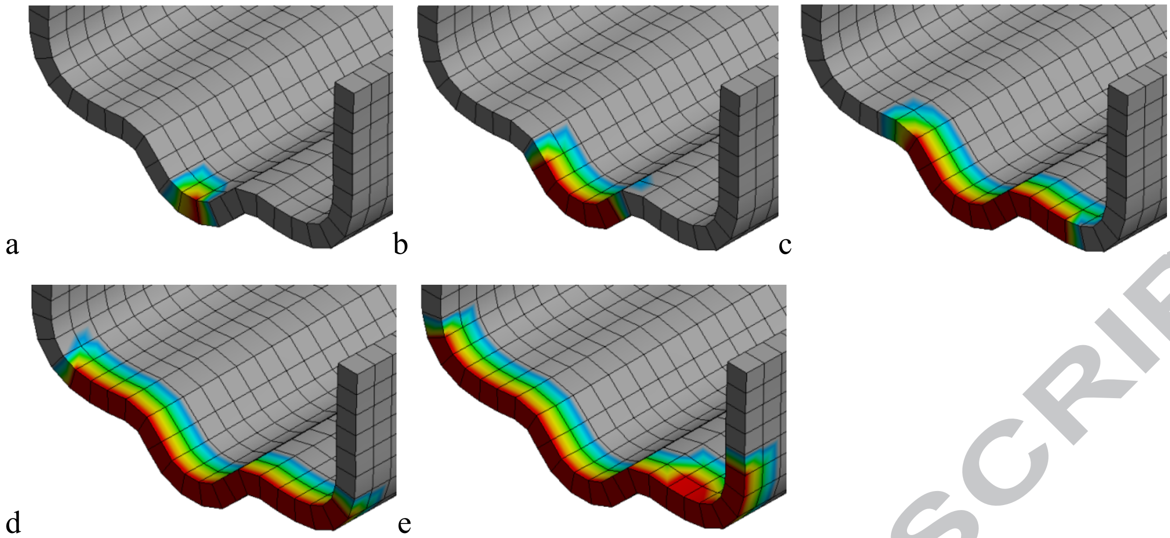

Figure 13: Exemplar progression of damage (jute 4 layers 2WS 1FS LL); a) 1.385kNm, b) 1.399kNm, c) 1.401kNm, d) 1.380kNm, e) 1.349kNm (red is fully damaged, grey is no damage)

TABLES

	E_T (MPa)	ε_{uT} (%)	f_{uT} (MPa)	f_{uC} (MPa)	f_{uS} (MPa)
Flax	6,386	1.1	55.1	61.5	33.0
Jute	6,941	1.5	62.1	51.3	34.2

Table 1: Measured material properties of the natural fibre composites (E_T is the elastic modulus in tension, ε_{uT} is the failure strain in tension, and f_{uC}, f_{uT} and f_{uS} are the ultimate compression, tension and in-plane shear stresses, respectively)

Fibre	Section	Fibre layers	Fibre weight (g/m^2)	D (mm)	B (mm)	L (mm)	t (mm)	I_{full} ($x10^3$) (mm^4)	E_T (MPa)	f_{uT} (MPa)	M_{test} (kNm)	f_{ult} (MPa)	I_{eff} ($x10^3$) (mm^4)	NA shift (mm)	M_{test} $/M_{Apred}$	M_{test} $/M_{FEpred1}$	M_{test} $/M_{FEpred2}$	N-M limit	M defl. (mm)
Jute	1WS, SL	4	1600	110.4	57.4	17.9	3.4	1478	6941	62.1	1.189	44.4	1344	3.4	1.01	0.97	0.97	0.84	13.3
Jute	1WS, LL	4	1600	110.9	58.2	27.2	3.4	1548	6941	62.1	1.229	44.0	1364	4.8	1.06	0.92	0.92	0.78	12.7
Jute	2WS, SL	4	1600	112.5	57.9	16.2	3.4	1546	6941	62.1	1.234	44.9	1439	2.6	0.98	0.98	0.98	0.87	12.7
Jute	2WS, LL	4	1600	112.0	57.8	26.4	3.4	1622	6941	62.1	1.301	44.9	1434	4.6	1.07	0.95	0.95	0.82	12.1
Jute	2WS, 1FS, SL	4	1600	109.9	57.3	16.2	3.4	1625	6941	51.9	1.109	37.5	1492	3.1	1.03	1.02	1.02	0.87	12.1
Jute	2WS, 1FS, LL	4	1600	109.2	57.4	26.8	3.4	1698	6941	51.9	1.043	33.5	1485	4.9	0.99	0.85	0.85	0.83	11.5
Jute	2WS, 1FS, SL	6	2400	115.1	61.3	16.6	5.5	2764	6941	62.1	2.216	46.1	2764	0.0	0.90	1.03	1.03	0.46	7.1
Jute	2WS, 1FS, LL	6	2400	115.0	61.4	25.8	5.5	2899	6941	62.1	2.511	49.8	2899	0.0	0.97	1.07	1.07	0.41	6.8
Flax	1WS, SL	4	1600	109.6	57.3	17.3	3.3	1434	6386	55.1	1.303	49.8	1354	2.2	0.92	1.12	1.01	0.82	14.8
Flax	1WS, LL	4	1600	109.9	57.5	27.7	3.3	1502	6386	55.1	1.351	49.4	1337	4.5	0.98	1.09	0.94	0.77	14.2
Flax	2WS, SL	4	1600	111.9	57.2	17.5	3.3	1501	6386	55.1	1.393	51.9	1429	2.8	0.94	1.16	1.05	0.79	14.2
Flax	2WS, LL	4	1600	111.0	57.7	27.0	3.3	1575	6386	55.1	1.447	51.0	1447	4.3	0.97	1.11	0.97	0.71	13.5
Flax	2WS, 1FS, SL	4	1600	108.8	57.1	15.4	3.3	1577	6386	55.1	1.355	46.7	1471	2.6	0.87	1.14	0.99	0.75	13.5
Flax	2WS, 1FS, LL	4	1600	108.4	57.0	25.2	3.3	1648	6386	55.1	1.501	49.4	1447	4.9	1.00	1.15	1.05	0.70	12.9
Flax	2WS, 1FS, SL	6	2400	113.5	59.8	15.7	5.1	2512	6386	55.1	2.184	49.3	2512	0.0	0.90	1.14	0.99	0.44	8.5
Flax	2WS, 1FS, LL	6	2400	114.0	60.1	24.2	5.1	2635	6386	55.1	2.489	53.8	2635	0.0	0.98	1.19	1.01	0.38	8.1
														Mean:	0.97	1.06	0.99		
														COV:	0.06	0.10	0.06		

Table 2: Natural fibre composite channel section dimensions and test results compared with analytical and finite element predictions (dimensions refer to Figure 3, M_{Apred} refers to analytically predicted values, M_{FEpred} refers to finite element predicted values, f refers to stress, M refers to moment, I refers to second moment of area, E_T is the tension elastic modulus) (WS is web stiffener, SL is shorter length flange edge stiffener, LL is longer length flange edge stiffener and FS is internal flange stiffener)

APPENDIX A

This Appendix describes the commercially produced fabrics used to fabricate the composite channel sections, and summarises relevant manufacturers data for the fabric and the epoxy used. The fabrics were commercially produced by Composites Evolution (compositesevolution.com), specifically for fibre-resin composites manufacture: Biotex Flax 400g/m^2 and Biotex Jute 400g/m^2. Both fabric products are a 2x2 Twill weave, which is a generic pattern consisting of bi-directional yarns woven over-over-under-under, where the yarns are perpendicular (i.e. 0º/90º), as demonstrated in Figure A1 (a). Examples of the commercial fabric are shown in Figure A1 (b, c). Composites Evolution provides technical data for the Biotex fabrics as summarised in Table A1. The commercial epoxy resin Kinetix R240 with H126 (fast) hardener was used for all composite fabrications. The epoxy is a room temperature out-of-autoclave cure epoxy resin that does not require heat input to cure. Kinetix provides technical data for Kinetix R240 with H126 as summarised in Table A2.

Figure A1: 2x2 Twill weave fabric: a) generic pattern, b) Biotex Jute 400g/m^2 c) Biotex Flax 400g/m^2

	Fabric	Yarn	Weight (g/m^2)	Density (g/cm^3)	Fibre tension strength (MPa)	Fibre tension modulus (GPa)	Typical composite fibre volume fraction* (%)	Typical composite tension strength* (MPa)	Typical composite tension modulus* (GPa)
Biotex Flax	2x2 Twill	Low-twist	400	1.5	500	50	30	72	8.5
Biotex Jute	2x2 Twill	Low-twist	400	1.46	400	40	29	59	8.1

* vacuum infused unsaturated polyester matrix

Table A1: Manufacturers' data for the Biotex fabrics

Pot Life - 100g @ 25ºC (in air)	20 minutes
Thin-laminate Open Time @ 25ºC	2 hours
De-mould time @ 25ºC	5 hours
Mix viscosity @ 25ºC	880 mPas
Shore D Hardness -1 day	79
Shore D Hardness – 2 weeks	82

Table A2: Manufacturers' data for Kinetix R240 with H126

APPENDIX B

This Appendix contains an example calculation of the moment capacity using AS/NZS4600 [27] and the procedures outlined in Section 4. Further examples of effective width calculations for natural fibre channels to AS/NZS4600 are provided in the supplementary file of [24]. The following calculation is for a four layered flax channel with one intermediate web stiffener and shorter flange edge stiffener (Figure B1, Table 2), with relevant notation:

b is the flat width of the flange, excluding the corner radii (*r*)
dL is the flat width of the flange edge stiffener, excluding the corner radii (*r*)
I_s is the second moment of area of the flange edge stiffener
I_a is the limit value for the second moment of area of the flange edge stiffener
k is the buckling factor of the flange
f_{cr} is the buckling stress of the flange
λ is the slenderness of the flange
ρ is the effectiveness factor of the flange
b_{eff} is the effective width of the flange
dL_{eff} is the effective width of the flange edge stiffener
E_C is the compression elastic modulus
f_{uC} is the maximum compression stress
f_{uT} is the maximum tension stress
I_{eff} is the effective section second moment of area
y_{eff} is the effective section neutral axis position
M_{Apred} is the analytically predicted moment capacity of the effective section

$$b = 57.3 - 2t - 2r = 57.3 - (2\ x\ 3.3) - (2\ x\ 6) = 38.7mm$$

$$dL = 17.3 - r - t = 17.3 - 6 - 3.3 = 8mm$$

$$S = 1.28\sqrt{\frac{E_C}{f_{uc}}} = 1.28\sqrt{\frac{4199}{61.5}} = 10.6$$

$$I_s = \frac{t\ x\ d_L^3}{12} = 141mm^3$$

$$I_a = 399t^4\left(\frac{b}{S\ x\ t} - 0.328\right) \leq t^4\left(\frac{115b}{S\ x\ t} + 5\right) = 15715mm^4$$

$$n = 0.582 - \frac{b}{4S\ x\ t} \geq 0.33 = 0.33$$

$$k = \left(\frac{I_s}{I_a}\right)^n \left(4.82 - \frac{5dL}{b}\right) + 0.43 = 0.97$$

$$f_{cr} = \frac{k\pi^2 E \quad t^2}{12(1-\upsilon^2)b^2} = 27MPa$$

$$\lambda = \sqrt{\frac{f_{uC}}{f_{cr}}} = 1.52$$

$$\rho = \frac{1.28}{\lambda^{1.5}} = 0.68$$

$$b_{eff} = \rho \; x \; b = 26.5mm$$

$$dL_{eff} = dL\frac{I_s}{I_a} = 0.1mm$$

The web is fully effective. The effective section was entered into the cross-section analysis software ThinWall, providing the following:

$I_{eff} = 1.354 \; x \; 10^6 \; \mathrm{mm}^4$

$y_{eff} = \frac{109.9}{2} - 2.2 = 52.6mm$ where the neutral axis shifted 2.2mm towards the tension side

$$M_{Apred} = \frac{f_{uT} I_{eff}}{y_{eff}} = \frac{55.1 \; x \; 1.354e^6}{52.6} = 1.42kNm$$

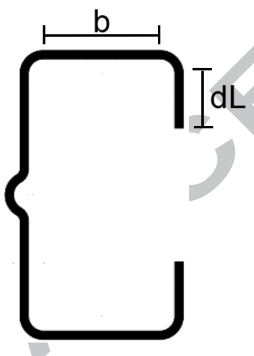

Figure B1: Flat widths of the flange (*b*) and flange edge stiffener (*dL*) of a channel with one intermediate web stiffener

APPENDIX C

	Jute	Flax	Units
Orthotropic elasticity			
Young's modulus X-direction	6941	6386	MPa
Young's modulus Y-direction	6941	6386	MPa
Young's modulus Z-direction	694	639	MPa
Poisson's ratio XY	0.29	0.26	
Poisson's ratio YZ	0.29	0.26	
Poisson's ratio XZ	0.29	0.26	
Shear modulus XY	2690	2534	MPa
Shear modulus YZ	269	253	MPa
Shear modulus XZ	269	253	MPa
Orthotropic stress limits			
Tensile X-direction	62.1	55.1	MPa
Tensile Y-direction	62.1	55.1	MPa
Tensile Z-direction	62.1	55.1	MPa
Compressive X-direction	-51.3	-61.5	MPa
Compressive Y-direction	-51.3	-61.5	MPa
Compressive Z-direction	-51.3	-61.5	MPa
Shear XY	34.2	33	MPa
Shear YZ	34.2	33	MPa
Shear XZ	34.2	33	MPa
Orthotropic strain limits			
All values	0.1	0.1	
Tsai-Wu constants			
All values	-1	-1	
Damage initiation criteria			
All values	Hashin	Hashin	
Damage evolution law			
G for tensile fibre damage	1.08	1.81[a]	N/mm
Damping for tensile fibre damage	0.1	0.1	
G for compressive fibre damage	1.08	1.81[a]	N/mm
Damping for compressive fibre damage	0.1	0.1	
G for tensile matrix damage	1.08	1.81[a]	N/mm
Damping for tensile matrix damage	0.1	0.1	
G for compressive matrix damage	1.08	1.81[a]	N/mm
Damping for compressive matrix damage	0.1	0.1	

[a] The modified value used to fit the experimental data was 5.43N/mm

Table C1: Material properties used in ANSYS finite element models